Journal for ImmunoTherapy of Cancer

Polymorphonuclear myeloid-derived suppressor cells and phosphatidylinositol-3 kinase gamma are critical to tobacco-mimicking oral carcinogenesis in mice

Khoa A Nguyen,[1] Lisa N DePledge,[1] Li Bian,[1] Yao Ke,[1,2] Von Samedi,[1] Amber A Berning,[1] Philip Owens,[1] Xiao-Jing Wang,[1,2] Christian D Young [1]

To cite: Nguyen KA, DePledge LN, Bian L, *et al*. Polymorphonuclear myeloid-derived suppressor cells and phosphatidylinositol-3 kinase gamma are critical to tobacco-mimicking oral carcinogenesis in mice. *Journal for ImmunoTherapy of Cancer* 2023;**11**:e007110. doi:10.1136/jitc-2023-007110

► Additional supplemental material is published online only. To view, please visit the journal online (http://dx.doi.org/10.1136/jitc-2023-007110).

Accepted 23 August 2023

[1]Department of Pathology, University of Colorado Anschutz Medical Campus, Aurora, Colorado, USA
[2]Department of Pathology & Laboratory Medicine, University of California Davis, Davis, California, USA

Correspondence to
Dr Christian D Young; christian.young@cuanschutz.edu

ABSTRACT

Background Oral squamous cell carcinoma (OSCC) is a devastating disease most often associated with tobacco consumption that induces a field of mutations from which a tumor arises. Identification of ways to prevent the emergence of cancer in high-risk patients is an ultimate goal for combatting all types of cancer, including OSCC.

Methods Our study employs a mouse model of tongue carcinogenesis induced by tobacco carcinogen mimetic, 4-nitroquinoline 1-oxide (4NQO), to establish tongue dysplasia and OSCC. We use conventional histology, immunohistochemistry, multispectral imaging, mass cytometry, novel cell lines, pharmaceutical inhibition of PI3Kγ, T-cell suppression assays and mouse transplant models in our functional experimentation.

Results In our study, we identify Ly6G+ granulocytes as the most abundant immune cell type in a model of tongue carcinogenesis induced by tobacco carcinogen mimetic 4NQO. Targeting Ly6G+ granulocytes with a pharmacologic inhibitor of PI3Kγ, an isoform of PI3K exclusively expressed by myeloid cells, resulted in reduced tongue dysplasia severity, and reduced rates of OSCC. Importantly, we performed functional assays with the Ly6G+ granulocytes induced in cell line models of 4NQO carcinogenesis to demonstrate that these granulocytes have increased polymorphonuclear myeloid-derived suppressor cells (PMN-MDSC) activity against T-cell proliferation and these PMN-MDSCs play a functional role in promoting tumor formation by inhibiting tumor regression in a PI3Kγ-dependent manner.

Conclusions Overall, our data suggest that recruitment of PMN-MDSCs to sites of dysplasia is critical to immune suppression of CD8 T cells, thereby permitting malignancy, and PI3Kγ inhibitors are one mechanism to reduce PMN-MDSC recruitment, immunosuppression and tumorigenesis in OSCC.

WHAT IS ALREADY KNOWN ON THIS TOPIC

⇒ Dysplasia progression to oral squamous cell carcinoma (OSCC) using the 4-nitroquinoline 1-oxide (4NQO) carcinogenesis model that closely mimics tobacco has been well established. Many of these studies have characterized the cells, genes and/or molecules present at different stages of pathology. Additionally, many studies pose therapies, cell types or genes regulating carcinogenesis in the 4NQO model.

WHAT THIS STUDY ADDS

⇒ Our study builds on this strong backbone of research by adding mechanistic characterization of granulocyte activities in the 4NQO carcinogenesis model and adding unique cell models of cancer and pre-cancer to determine the role of polymorphonuclear myeloid-derived suppressor cells (PMN-MDSCs) and PI3Kγ in regulating progression to malignancy.

HOW THIS STUDY MIGHT AFFECT RESEARCH, PRACTICE OR POLICY

⇒ Our study offers insight into PMN-MDSCs and PI3Kγ as microenvironmental regulators of malignancy, thereby supporting further investigation into the use of PMN-MDSCs and PI3Kγ as predictive biomarkers in matching patients to rational therapies as well as the functional targeting of these regulators of immunosuppression.

BACKGROUND

Head and neck squamous cell carcinoma (HNSCC) is the sixth most common cancer type, accounting for over 890,000 new cases and approximately 450,000 deaths annually worldwide.[1 2] This malignancy and its treatments have severe impacts on quality of life of patients and a 5-year survival rate of about 60%.[3] As these cancers and their localized treatments (surgery and radiation) occur in sensitive areas of the oral and nasal cavities including the tongue, jaw, airways, etc, it is common for patients to incur impairments in speech, swallowing, taste, chewing, along with potential facial disfigurement, and psychological distress. While immune checkpoint

inhibitor therapies have improved patient outcomes[4 5] and quality of life,[6] identifying mechanisms to intervene early in carcinogenesis and spare patients from cancer and its treatments would be revolutionary.

HNSCC originates from stratified epithelium and progresses through stages of dysplasia, carcinoma in situ and ultimately invasive carcinoma. Dysplasia severity is highly correlated with risk of malignant progression.[7] Major risk factors for this disease include tobacco use and human papillomavirus (HPV) infection, of which the former faces a much worse prognosis even when treated with radio-chemotherapy.[3 8 9] In contrast to HPV-related HNSCC, tobacco-related oral SCC (OSCC) risk can be associated with "oral potentially malignant disorders" (OPMD), which most commonly appear as white or red patches on the oral mucosa, known as leukoplakia or erythroplakia, respectively.[10] While most patients with OSCC present without a documented history of OPMD,[3] the estimated worldwide OPMD prevalence is 4.5% with malignant transformation rates of 8.6% and 33.1% for leukoplakia and erythroplakia, respectively.[10 11] This leaves a large population of identifiable individuals at risk of malignant progression.

Breakthrough discoveries in immune-focused therapies for cancer highlight the potency of leveraging the immune system to treat cancer.[12 13] While the premalignant environment has been reported to be proinflammatory, malignant cells eventually overcome host inflammatory response by mediating immune escape.[14 15] The underlying mechanisms facilitating immune escape in the transition from premalignancy to HNSCC therefore represent an attractive therapeutic target in cancer chemoprevention. Indeed, immune checkpoint blockade (ICB) has been shown to prevent malignant progression of dysplasia to OSCC in a mouse model of carcinogenesis.[16] Identifying major mechanisms of immunosuppression in premalignancy is therefore critical in the development of therapeutic strategies to halt malignant transformation, thereby sparing patients from both cancer and its treatments. One such mechanism of immunosuppression is the PI3K signaling pathway, as recent reports suggest a critical role of a myeloid cell specific PI3K enzyme, PI3Kγ, in promoting immunosuppression via protumor activity of M2 macrophages and immunosuppressive myeloid-derived suppressor cells (MDSCs) in HNSCC and other cancer types.[17 18] Thus, it stands to reason that the PI3Kγ signaling pathway is also involved in immunosuppression of premalignant lesions prior to malignant transformation and may be a promising therapeutic target for OPMDs or other high-risk patients, although this is less studied.

The 4-nitroquinoline 1-oxide (4NQO) mouse model of oral carcinogenesis is well suited for studying immune changes during carcinogenesis as it mimics the effects of tobacco, recapitulates the histological progression of dysplasia to invasive carcinoma, undergoes immune cell infiltration, and produces tumors closely resembling human OSCC etiology and mutational landscape.[19–22] Studies have shown that 4NQO carcinogenesis produces mutations ~94% similar to the tobacco induced mutation signature observed in human patients and induces mutations in genes frequently mutated in tobacco-associated HNSCC, altogether making 4NQO a widely accepted, robust model of tobacco-associated OSCC.[20 22] In the present study, we used the 4NQO carcinogenesis protocol to investigate opportunities to intervene in progression of dysplasia to OSCC and identify functional mechanisms that drive malignancy. We observed significantly increased levels of systemic and tongue-localized granulocytes in mice during carcinogenesis, as reported previously.[20 23] Thus, we hypothesized that granulocytes may confer immunosuppressive properties in premalignant lesions, thereby facilitating immune escape and carcinogenesis. We demonstrated that inhibition of PI3Kγ reduced granulocytes at sites of dysplasia, lessened the severity of dysplasia and diminished the emergence of invasive OSCC. We showed that granulocytes from this model function as MDSCs to suppress T-cell proliferation and these MDSCs enable the engraftment of a poorly tumorigenic, 4NQO-derived cancer cell line. In our model of PI3Kγ inhibition, which reduces granulocyte recruitment, HNSCC engraftment is rejected. Taken together, our study provides novel insights and functional validation to demonstrate the critical role of polymorphonuclear MDSCs (PMN-MDSCs) and PI3Kγ in immune suppression. Thus, our studies highlight the role of PMN-MDSCs and PI3Kγ in permitting the progression of HNSCC and suggest novel targets for chemoprevention of HNSCC.

METHODS

Reagents

4NQO (Sigma) was dissolved in propylene glycol (Sigma) at a stock concentration of 5 mg/mL and then diluted 1:100 in water for the working concentration, 50 µg/mL. IPI549 was purchased from MedChemExpress. Polyethylene glycol 300 (PEG300) and dimethyl sulfoxide (DMSO) were purchased from Sigma. Cell culture media (Dulbecco's Modified Eagle Medium: Nutrient Mixture F12 (DMEM/F12) and keratinocyte media) were purchased from Life Technologies. Fetal bovine serum (FBS) was purchased from Seradigm or Life Technologies. Primocin was purchased from InvivoGen. Matrigel was purchased from Corning. Taqman gene expression assays used in this study are detailed in online supplemental table S1. Antibodies used in this study are detailed in online supplemental tables S2 and S3.

4NQO model of HNSCC carcinogenesis and treatments

4NQO was diluted to 50 µg/mL in the drinking water of 6–8 weeks old female C57BL/6J mice and provided ad libitum for 16 or 18 weeks (as indicated) after which mice were provided regular drinking water.[19 20] Mice were euthanized at the indicated times for complete blood count (CBC), histology, flow/mass cytometry and

cell line establishment as described below. IPI549 was dissolved in DMSO to 100 mg/mL, then diluted to the working concentration (~2.7–3.7 mg/mL depending on mouse weight) using PEG300 (Sigma). An equal ratio of DMSO to PEG300 was used as vehicle control. IPI549 (or vehicle control) was administered in 100 µL volume by oral gavage daily, 6 days per week, for a dose of 15 mg drug/kg mouse weight (eg, 100 µL of 3 mg/mL IPI549 to a 20 g mouse). Animals were euthanized at the indicated time points and tongues harvested for gross examination, histology, or mass cytometry.

Cell line generation, daughter cell line generation and transplantation

Tongues of mice ~26 weeks post-4NQO initiation were split in half longitudinally, with half fixed in 10% neutral buffered formalin for paraffin embedding and histology analyses, and the other half placed into DMEM for generating cell lines. Details of cell line generation are described in online supplemental materials and methods. A1206 and A1207 tongue tumor cell lines were established from different 4NQO-treated mice. For transplantation in experiments, 1 million cells were transplanted in 100 µL volume (50% Matrigel, 50% phosphate-buffered saline (PBS)) to the flank of recipient female C57BL/6J mice or 0.25 million cells transplanted in 25 µL volume (50% Matrigel, 50% PBS) to the dorsal tongue of recipient C57BL/6J mice. Granulocytes were co-transplanted as indicated. Wild type and tumor bearing mice were harvested at the indicated time points for evaluation of tumors or harvest of leukocyte populations from spleens for functional assays.

Complete blood count and plasma isolation

Blood was collected to EDTA blood tubes by cardiac puncture immediately after euthanasia. CBC was analyzed on a Heska HemaTrue impedance analyzer at the University of Colorado Comparative Pathology Shared Resource using HeskaView and proprietary software. The remaining blood was centrifuged at 1500×g for 10 min and the liquid plasma portion was collected to a new tube and stored at −80°C.

Histology, dysplasia scoring, immunohistochemistry and multispectral imaging (MSI)

The 5 µm tissue sections on glass slides were dewaxed and hydrated using xylenes and graded alcohols, stained with H&E following standard techniques or immunohistochemistry (IHC)/multispectral imaging (MSI) stained as described in online supplemental materials and methods. Dysplasia in tongue sections was scored following 2017 WHO guidelines (normal, mild, moderate or severe; given numeric scores of 0, 1, 2 or 3, respectively)[7] by treatment-blinded pathologists and scores for each sample averaged. Whole slide scanning of H&E stained or IHC stained slides was performed using an Aperio XT scanner at the University of Colorado Pathology Shared Resource and analyzed using ImageScope software. Ly6G IHC staining was quantified by collecting five representative hotspot images at 20× magnification using the Aperio XT scanner and counted using Akoya Bioscience's inForm tissue analysis software to count the number of positively stained cells. MSI staining and image capture was performed at Human Immune Monitoring Shared Resource within the University of Colorado Human Immunology and Immunotherapy Initiative and is described in online supplemental materials and methods.

Gene expression and cytokine array analyses

Gene expression was analyzed by reverse transcriptase quantitative polymerase chain reaction (RT-qPCR) using standard techniques described in online supplemental materials and methods. Cell culture supernatant or plasma collected from mice was diluted and analyzed for cytokines, growth factors and chemokines using Proteome Profiler Mouse XL Cytokine Array (R&D Systems) following manufacturer's instructions and analyzed with QuickSpots software.

Leukocyte isolation, T-cell suppression and flow cytometry

Harvested spleens were minced with a sterile scalpel, transferred to a 100 µm strainer, smashed through with a syringe plunger, rinsed in PBS, and then pelleted by centrifugation. Tumor harvest, mechanical and enzymatic dissociation, red blood cell (RBC) lysis, DNase treatment and counts were performed as described in online supplemental materials and methods. Leukocyte populations were isolated using magnetic beads: CD8a T cells were isolated using Miltenyi Biotec CD8a+ T cell isolation kit (#130-104-075) and Ly6G+ cells were isolated using Miltenyi Biotec Myeloid-Derived Suppressor Cell Isolation kit (#130-094-538; using only the anti-Ly6G+ magnetic beads steps) following manufacturer's instructions. In total, 0.5 million cells from pre-isolation and post-isolation cell populations had their fragment crystallizable (FC) receptors blocked with FC blocking antibody and stained for myeloid cell populations (online supplemental table S2) then analyzed on the ZE5 Bio-Rad cell analyzer at the University of Colorado Flow Cytometry Shared Resource to validate enrichment of Ly6G+ cells. For T-cell suppression assays, isolated CD8+ T cells were labeled with carboxyfluorescein succinimidyl ester (CFSE) or CellTrace Violet (Thermo Scientific) following manufacturer's instructions and 1.5×10^5 were seeded per well of flat bottom 96 well plates in Roswell Park Memorial Institute Medium (RPMI)+10% FBS + 50 U/mL interleukin 2 (IL-2). T cells were stimulated with 1.5×10^5 anti-CD3/anti-CD28 Dynabeads (Invitrogen) and negative control wells were not stimulated. Isolated granulocytes were serially diluted twofold and added to wells at ratios of 1:1, 1:2, 1:4, 1:8, 1:16 or 0:1 MDSC:T cell and incubated for 3 days. T-cell proliferation was assessed by adding Ghost Dye Red 780 viability stain (Tonbo) and determining the dilution of CFSE or CellTrace Violet to determine proliferating and non-proliferating T cells

by flow cytometry on a ZE5 Bio-Rad cell analyzer at the University of Colorado Flow Cytometry Shared Resource.

Mass cytometry

Tumors were harvested from euthanized mice, dissociated to single cells, stained with metal-tagged antibodies detailed in online supplemental table S3 and analyzed as described in online supplemental materials and methods. Cells were analyzed on a Helios mass cytometer (Fluidigm) at the University of Colorado Flow Cytometry Shared Resource, and normalized FCS files were uploaded to Cytobank (Cytobank) for statistical analysis. Positive staining for cisplatin was used to exclude dead cells, and nucleated cells were confirmed with IR-Dye (Fluidigm). Live, nucleated CD45+ cells were clustered using Cytobank's viSNE dimensionality reduction analysis with number of iterations set to 1,000, perplexity set to 30, and Theta set to 0.5. The resulting viSNE plots were then gated based on marker expression.

Statistics

Statistics were performed using GraphPad Prism software. Two groups were compared using unpaired Student's t-test, unless otherwise indicated. Comparison of more than two groups was performed by one-way analysis of variance (ANOVA) (one variable) or two-way ANOVA (two variables) with Tukey's multiple comparison test. Survival analysis was performed using the log-rank (Mantel-Cox) test.

RESULTS

Granulocytes are increased in the tongues and blood of mice treated with tobacco-mimicking carcinogenesis protocol

We used the 4NQO carcinogenesis protocol that causes DNA damage and mutations in the tongues of mice, resulting in dysplasia that can progress to OSCC.[19 20] Importantly, the mutational signature and histopathological progression of 4NQO-induced tumors in mice closely mirrors that of human tobacco-induced OSCC.[20 22] To study the process of OSCC initiation and progression, we treated mice with 4NQO and observed them over a period of 26–28 weeks. H&E-stained sections of mouse tongues at weeks 12, 15, and 26–28 revealed a steady progression from normal tissue to mild/moderate dysplasia to severe dysplasia and, finally, to SCC (figure 1A,B). To determine systemic immune cell changes during carcinogenesis, we performed CBC analysis of blood at time points 12, 15, and 26–28 weeks. We found significantly increased levels of total white blood cells, monocytes, and granulocytes in 4NQO-treated mice compared with water-treated control mice at the 28-week time point, while levels of lymphocytes and monocytes were decreased at 12 weeks in 4NQO-treated mice (figure 1C). To characterize local immune cell changes, we used a six-color MSI panel staining for E-cadherin, Gr1, F4/80, B220, CD3ε, and DAPI in the tongues of mice to identify epithelial cells, granulocytes/monocytes, macrophages, B lymphocytes, T lymphocytes and nuclei, respectively. We found the levels of Gr1+ infiltrate were significantly higher at the 28-week 4NQO time point compared with 12-week and 15-week time points, and Gr1+ cells were the most abundant immune cell type observed in mouse tongues regardless of pathology (figure 1D,E). Because Gr1 can stain both monocytes and granulocytes, we analyzed single cell suspensions of dissociated mouse tongues and found that Ly6G+ granulocytes, but not Ly6C+ monocytes, were increased in mice undergoing 4NQO carcinogenesis compared with water treated controls (online supplemental figure S1). Comparing regions of mild, moderate, and severe dysplasia, we observed the highest levels of Gr1+ cells in regions of severe dysplasia (figure 1F). Because we observed elevated granulocytes in blood and in sites of dysplasia in 4NQO-treated mice we next used the plasma of mice treated with water or 4NQO harvested at 15 or 28 weeks, time points representing mild dysplasia and severe dysplasia/SCC, respectively, for cytokine array analysis. We focused on growth factors that stimulate granulopoiesis (Gcsf and Gmcsf) and chemokines that recruit granulocytes (Cxcl1, Cxcl2, Cxcl5).[24 25] This analysis demonstrated that 4NQO-treated mice had elevated levels of Cxcl1, Cxcl2 and Cxcl5 and modestly increased levels of Gmcsf (online supplemental figure S2) at the 28-week time point, suggesting these factors may play a role in increasing granulocyte production and homing to sites of severe dysplasia. Elevated Mpo, an enzyme uniquely expressed by granulocytes, correlated with increased systemic granulocytes (online supplemental figure S2). As granulocytes were increased systemically in mice with severe tongue dysplasia or SCC, were the most abundant immune cells locally, and correlated with severe dysplasia, our data suggests granulocytes play a causal role in pathogenesis.

Inhibition of p110γ reduces tobacco-mimicking carcinogenesis and granulocyte infiltration

PI3Kγ (catalytic subunit expressed from *PIK3CG* gene) is expressed exclusively in leukocytes,[26 27] thus its expression is restricted to blood and lymphoid organs (eg, spleen) unlike the ubiquitously expressed PI3Kα isoform (catalytic subunit expressed from *PIK3CA* gene). This was confirmed by gene expression analysis of publicly available data (online supplemental figure S3A,B) and immunoblot analysis comparing lysates of mouse OSCC cells to mouse splenocytes (online supplemental figure S3C). IPI549 is a small molecule PI3Kγ inhibitor shown to inhibit myeloid cell immunosuppression.[17 28] To determine whether PI3Kγ-expressing myeloid cells play a causal role in carcinogenesis, we administered IPI549 daily to mice after 18 weeks of 4NQO carcinogenesis (figure 2A), as this is the latest time point where moderate–severe dysplasia can be seen, but carcinoma is infrequent and allows 4weeks of treatment (up to week 22, when SCCs are known to emerge in untreated animals).[29] We found that mice treated with IPI549 had reduced numbers of gross exophytic lesions (figure 2B). Through

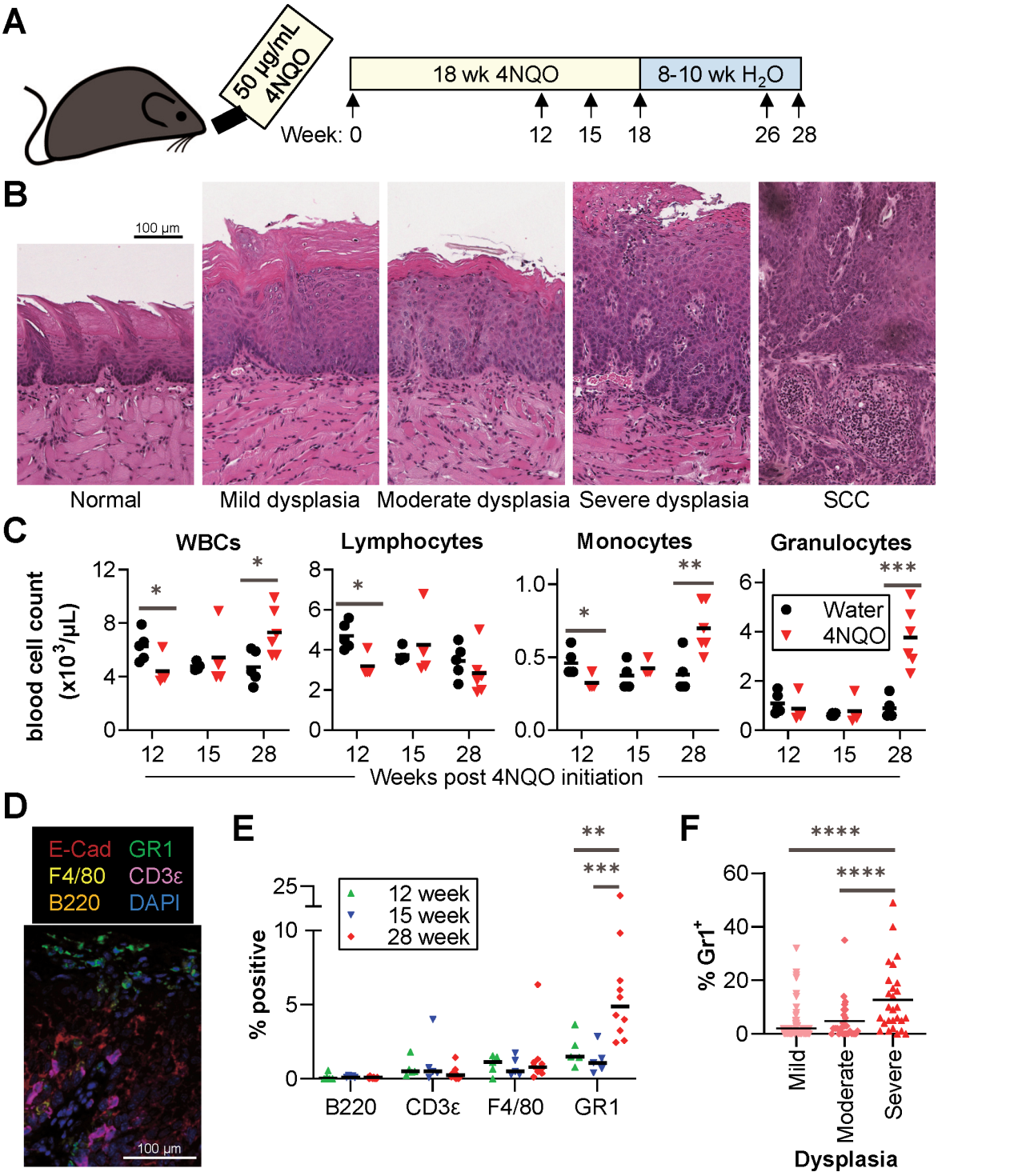

Figure 1 High levels of granulocytes in the tongues and blood of mice treated with tobacco-mimicking carcinogenesis protocol. (A) 4NQO carcinogenesis protocol: mice received 50 µg/mL 4NQO in the drinking water for 18 weeks and returned to regular drinking water thereafter. Mice were sacrificed at 12, 15 and 26–28 weeks post-4NQO initiation. (B) Representative images of normal tongues (dorsal surface) and tongues with dysplasia (mild, moderate and severe) or SCC resulting from 4NQO carcinogenesis. (C) Complete blood count of blood harvested from mice as described in panel A. *p<0.05, **p<0.01, ***p<0.001, determined by unpaired Student's t-test. (D–F) Multispectral imaging of immune cell markers. E-Cadherin (E-Cad) marks epithelial cells. F4/80 marks macrophages. B220 marks B lymphocytes. GR1 marks granulocytes and monocytes. CD3ε marks T lymphocytes. DAPI marks nuclei. (D) Representative image of multiple immune cell types in a dysplastic tongue. (E) The percentage of each immune cell type per mouse tongue harvested at the indicated time point (averaged from 8 to 14 fields of view per mouse). (F) The percentage of $GR1^+$ cells per field of view as a function of dysplasia severity in that field. **p<0.01, ***p<0.001, ****p<0.0001 determined by two-way ANOVA (panel E) or one-way ANOVA (panel F) with Tukey's multiple comparison test. ANOVA, analysis of variance; SCC, squamous cell carcinoma; WBCs, white blood cells; wk, week; 4NQO, 4-nitroquinoline 1-oxide.

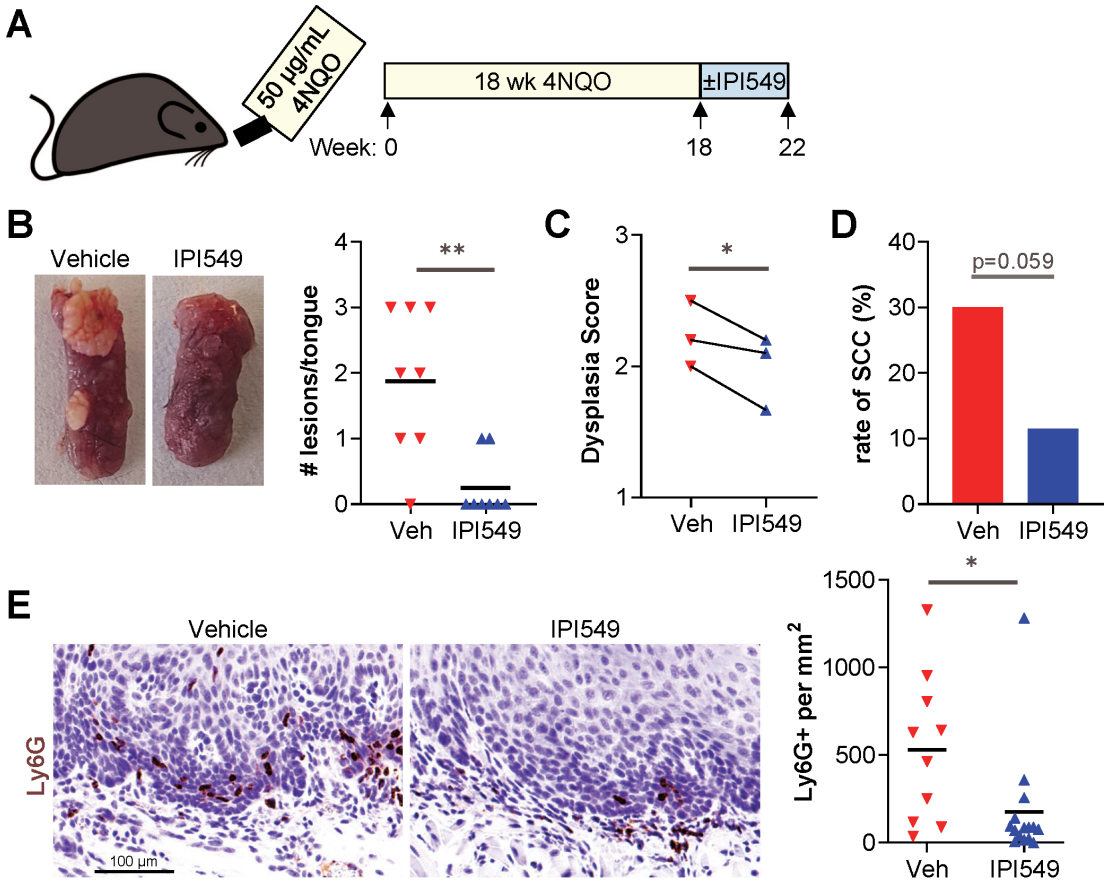

Figure 2 Inhibition of p110γ reduces tobacco-mimicking carcinogenesis and reduces granulocyte infiltration. (A) 4NQO carcinogenesis and treatment regimen: mice received 50 µg/mL 4NQO in the drinking water for 18 weeks and returned to regular drinking water thereafter. Mice received IPI549 or vehicle treatment for the final 4 weeks. (B) Representative gross images of tongues from mice treated with vehicle or IPI549 (left). Quantification of gross, exophytic lesions per tongue (right; **p<0.01 determined by unpaired Student's t-test). (C) The carcinogenesis and treatment protocol described in A was carried out three times and pathology scored by two treatment-blinded pathologists. Mild, moderate, or severe dysplasia was assigned a score of 1, 2 or 3, respectively. The average dysplasia score of three to six animals per group is presented across all three experiments (*p<0.05 determined by paired Student's t-test). (D) The rate of SCC malignancy at week 22 across all three experiments (analyzed by χ^2 analysis). (E) Representative Ly6G immunostaining and quantification across all three experiments. *p<0.05 determined by unpaired Student's t-test. SCC, squamous cell carcinoma; wk, week; 4NQO, 4-nitroquinoline 1-oxide.

scoring of tongue dysplasia by two board certified pathologists blinded to treatment in three independent repeats of this experiment, we observed a reduction in severity of dysplasia as well as reduced SCC formation in mice treated with IPI549 compared with vehicle (figure 2C,D). To determine whether IPI549 affected granulocyte infiltrate, we performed IHC to quantify the abundance of Ly6G+ cells at sites of dysplasia and/or SCC and found significantly diminished Ly6G+ density in mice treated with IPI549 compared with vehicle (figure 2E). Mass cytometry analysis of dissociated tongue tissue demonstrated similar results: Ly6G+ granulocyte abundance, but not Ly6C+ monocyte abundance, was decreased in 4NQO-treated mice treated with IPI549 as compared with vehicle treated mice (online supplemental figure S1).

Tumorigenic tongue SCC cell lines have increased granulocytes and reduced activated CD8+ T cells early in tumorigenesis

We developed syngeneic, transplantable OSCC cell lines, A1206 and A1207, from two independent 4NQO-treated mouse tongues (figure 3A). Transplantation of A1206 cells into the flanks of immunocompetent C57BL/6 mice led to tumor formation in 100% of recipient mice with tumors reaching 1000 mm^3 in ~8 weeks (figure 3B, left panel). However, A1207 cells formed tumors in ~20% of C57BL/6 recipients and required >25 weeks to reach 500 mm^3 (figure 3B, middle panel). This contrasts with the 100% tumor formation rate of A1207 cells transplanted into immune compromised nude mice (figure 3B, middle panel, blue lines) or the 100% tumor formation rate of A1207 tumor fragments transplanted into C57BL/6 mice (figure 3B, right panel). Additionally, in mice bearing tumors established from A1207 cells or A1207 tumor fragments, lung metastasis is observed in >90% of animals (figure 3C), suggesting that, once established, A1207 is an aggressive OSCC model.

Since A1207 cells are poorly tumorigenic but A1207 tumor fragments are highly tumorigenic, it suggested microenvironmental factors contained within the tumor rather than the tumor cells are critical for A1207

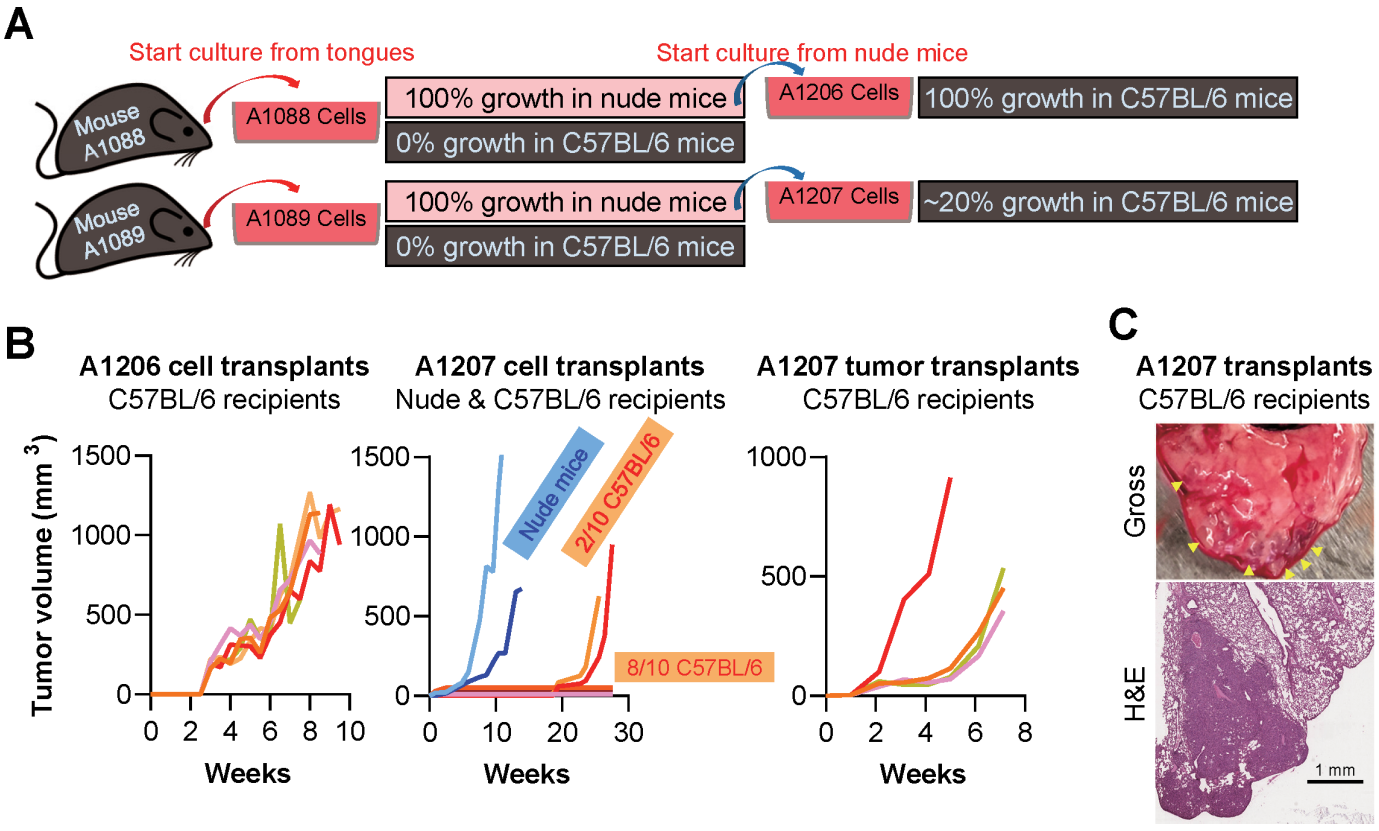

Figure 3 Establishing tumorigenic tongue SCC cell lines. (A) A1088 and A1089 cell lines were established independently from the tongues of two different 4NQO-treated mice. A1206 and A1207 cell lines were established from nude mouse tumors initiated by A1088 and A1089 cells, respectively. (B) The tumor growth rate of A1206 cells, A1207 cells or A1207 tumor fragments in recipient C57BL/6 or nude mouse recipients. (C) Representative gross image and H&E-stained section of lungs from a mouse bearing A1207 tumor demonstrating lung metastasis. Yellow arrowheads point to grossly visible metastases. SCC, squamous cell carcinoma; 4NQO, 4-nitroquinoline 1-oxide.

tumorigenesis. In tumors initiated from A1207 cell transplants, we noted that tumor regression begins ~10 days post-transplant (figure 4A left panel). We used mass cytometry to evaluate the tumor immune microenvironment (TIME) of both A1206 and A1207 cell transplants 13 days post-transplant, prior to full A1207 tumor regression, but when A1207 tumors were regressing and smaller than A1206 tumors (figure 4A). We applied t-distributed stochastic neighbor embedding (t-SNE) analysis to compare CD45+ cells from A1206 versus A1207 transplants. A1207 transplants had lower levels of CD4+CD25+ regulatory T-cells. Remarkably, A1207 tumors had virtually no Ly6G+ granulocyte infiltrate compared with A1206 tumors (figure 4B). RNA harvested from A1206 and A1207 tumor cell lines in vitro demonstrated that poorly tumorigenic A1207 cells express much less *Cxcl1*, *Cxcl2*, *Cxcl3* and *Cxcl5* (encoding chemokines that recruit granulocytes) and less *Csf3* and *Csf2* (encoding Gcsf and Gmcsf growth factors, respectively, that stimulate granulopoiesis) (online supplemental figure S4A). Cytokine array analysis of cell culture supernatants demonstrated that A1207 supernatants contain less Gcsf and Cxcl2 protein than A1206 (online supplemental figure S4B,C) suggesting that the lack of these factors may explain the lack of granulocytes in A1207 transplanted tumor cells. CD8+ T cell levels were much higher in A1207 transplants than in A1206 transplants (figure 4B). The levels of factors associated with cytotoxic T-cell activation (Tnfα, Ifnγ and Gzmb) were much higher in the CD8+ T cells of A1207 tumors than the CD8+ T cells of A1206 tumors (figure 4C). Together these data suggest that early after transplant, A1207 tumor cells fail to recruit immunosuppressive granulocytes and regulatory T cells, while also exhibiting higher levels of activated CD8+ T cells that may initiate tumor regression.

Tumorigenic tongue SCC cell lines have increased PMN-MDSCs

Using mass cytometry, we next addressed the TIME of established tumors (~500–800 mm^3 in volume). We used t-SNE analysis to compare CD45+ cells from A1206, A1207, and A223 tumors. In contrast to the A1206 and A1207 tumor lines induced by 4NQO carcinogenesis, A223 is a mouse SCC cell line initiated by activation of oncogenic $Kras^{G12D}$ and deletion of the Smad4 tumor suppressor in a genetically engineered mouse model of cancer.[30 31] Interestingly, tumors established from both 4NQO-derived cell lines, A1206 and A1207, showed significantly higher levels of Ly6G+ granulocyte infiltrate than A223 tumors (figure 5A). This demonstrated that, if established, A1207 tumors indeed contain

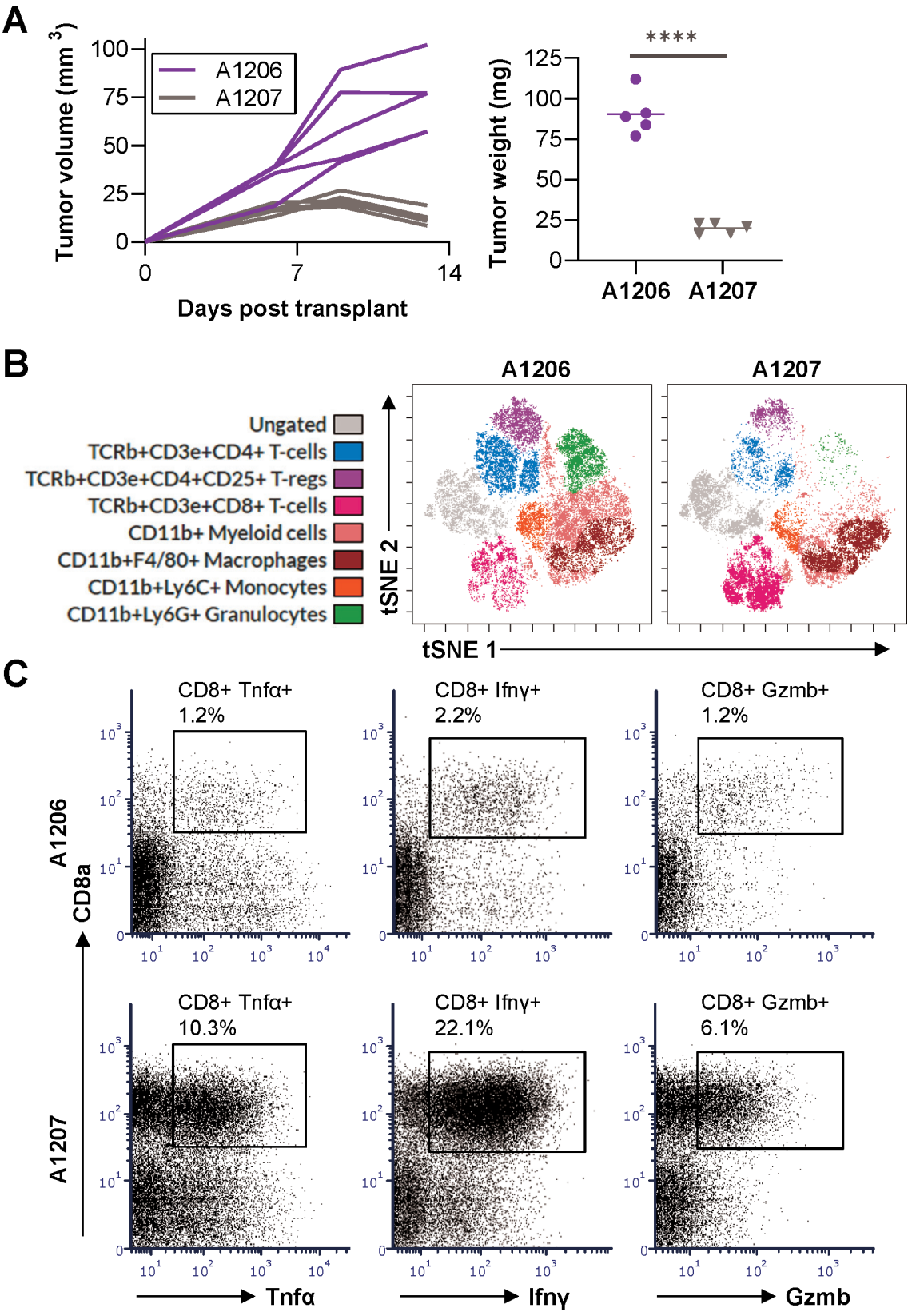

Figure 4 A1207 tumor regression is associated with scant granulocytes and increased activated CD8 T cells. (A) A1206 or A1207 cells were transplanted into C57BL/6 mice and size monitored for 13 days. On day 13, mice were sacrificed and tumors weighed. ****p<0.0001, determined by unpaired Student's t-test. (B–C) Twelve A1206 and 12 A1207 tumors were dissociated 13 days after implantation, the cells pooled, processed and stained for CyTOF analysis (using antibody panel 2) as described in methods. (B) tSNE analysis was performed to identify immune cell clusters in A1206 and A1207 tumors. (C) The live, $CD45^+$, $CD8^+$ population were further analyzed for levels of Tnfα, Ifnγ and Gzmb to determine $CD8^+$ T-cell activation. t-SNE, t-distributed stochastic neighbor embedding.

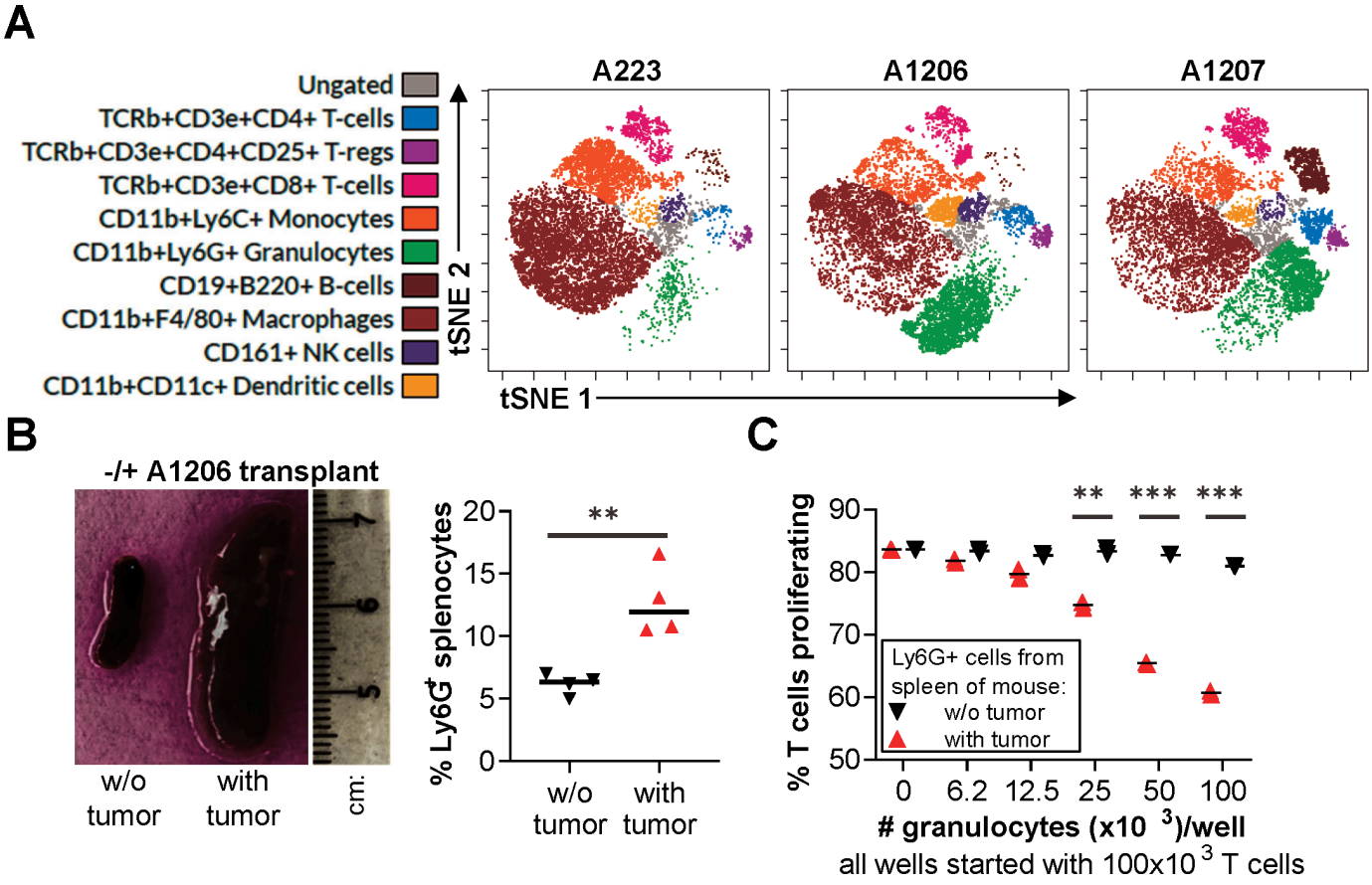

Figure 5 Tumorigenic tongue SCC cell lines have increased systemic PMN-MDSCs. (A) Transplanted A223, A1206 and A1207 tumors (~1000 mm^3) were harvested from C57BL/6 mice, dissociated and stained for CyTOF analysis using antibody panel 1. tSNE analysis was performed to identify immune cell clusters in A223, A1206 and A1207 tumors. (B) Representative image of spleens from a wild-type C57BL/6 mouse and a C57BL/6 mouse bearing an A1206 tumor (left). The percentage of Ly6G+ cells in spleens from C57BL/6 mice without tumors or with A1206 tumors (right). (C) Ly6G+ cells isolated from the spleen of a C57BL/6 mouse without a tumor or the spleen of a mouse bearing an A1206 tumor were co-cultured with CD8+ T cells isolated from a naïve mouse at the indicated cell number to determine whether Ly6G+ cells suppress T-cell proliferation (induced by IL-2 and anti-CD3, anti-CD28 beads). Representative data of three independent repeats. **p<0.01, ***p<0.001 as determined by Student's t-test. IL, interleukin; PMN-MDSCs; polymorphonuclear MDSCs; SCC, squamous cell carcinoma; t-SNE, t-distributed stochastic neighbor embedding.

high levels of granulocytes. Increased levels of granulocytes in a tumor are likely to act as immunosuppressive PMN-MDSCs, but this can only be assessed in functional assays that demonstrate suppressor function.[32] To address whether the Ly6G+ cells from our model are immunosuppressive, we performed a T-cell proliferation assay with co-cultured Ly6G+ cells harvested from spleens of un-transplanted or A1206-transplanted mice. We noted that the spleens of A1206 transplanted mice are significantly larger and contain a much higher percentage of Ly6G+ cells than spleens of wild-type control mice (figure 5B). We found that when Ly6G+ cells from non-tumor bearing mice are co-cultured with activated T-cells, there is no change in T-cell proliferation. In contrast, Ly6G+ cells isolated from spleens of A1206 tumor-bearing mice reduced T-cell proliferation in a cell number dependent manner (figure 5C; online supplemental figure 5). Together, these data suggest that the high population of Ly6G+ cells observed systemically in tumor-bearing mice from the 4NQO model are immunosuppressive and function as PMN-MDSCs.

Carcinogenic and immunosuppressive microenvironments enable A1207 p110γ-dependent tumor growth

Because we observed low levels of Ly6G+ infiltrate in regressing A1207 transplants and a high population of Ly6G+ infiltrate in successful A1207 transplants, we reasoned that microenvironmental Ly6G+ cells are critical for immunosuppression and tumorigenesis in this model. To test this, we performed orthotopic transplants of A1207 cells into tongues of mice treated with 4NQO for 16 weeks, a time at which dysplasia and granulocytes are increased, and into the tongues of control mice treated with water instead of 4NQO. Additionally, we treated a cohort of mice with IPI549 to test whether p110γ inhibition would affect A1207 tumorigenesis in 4NQO-treated mice. After allowing 4 weeks for transplants to establish and respond to vehicle or IPI549 treatments, we harvested tongues from mice for histological analysis (figure 6A). Tumors resulting from A1207 transplant are well-circumscribed in the muscle of the tongue and easily distinguished from the occasional SCC induced by 4NQO at

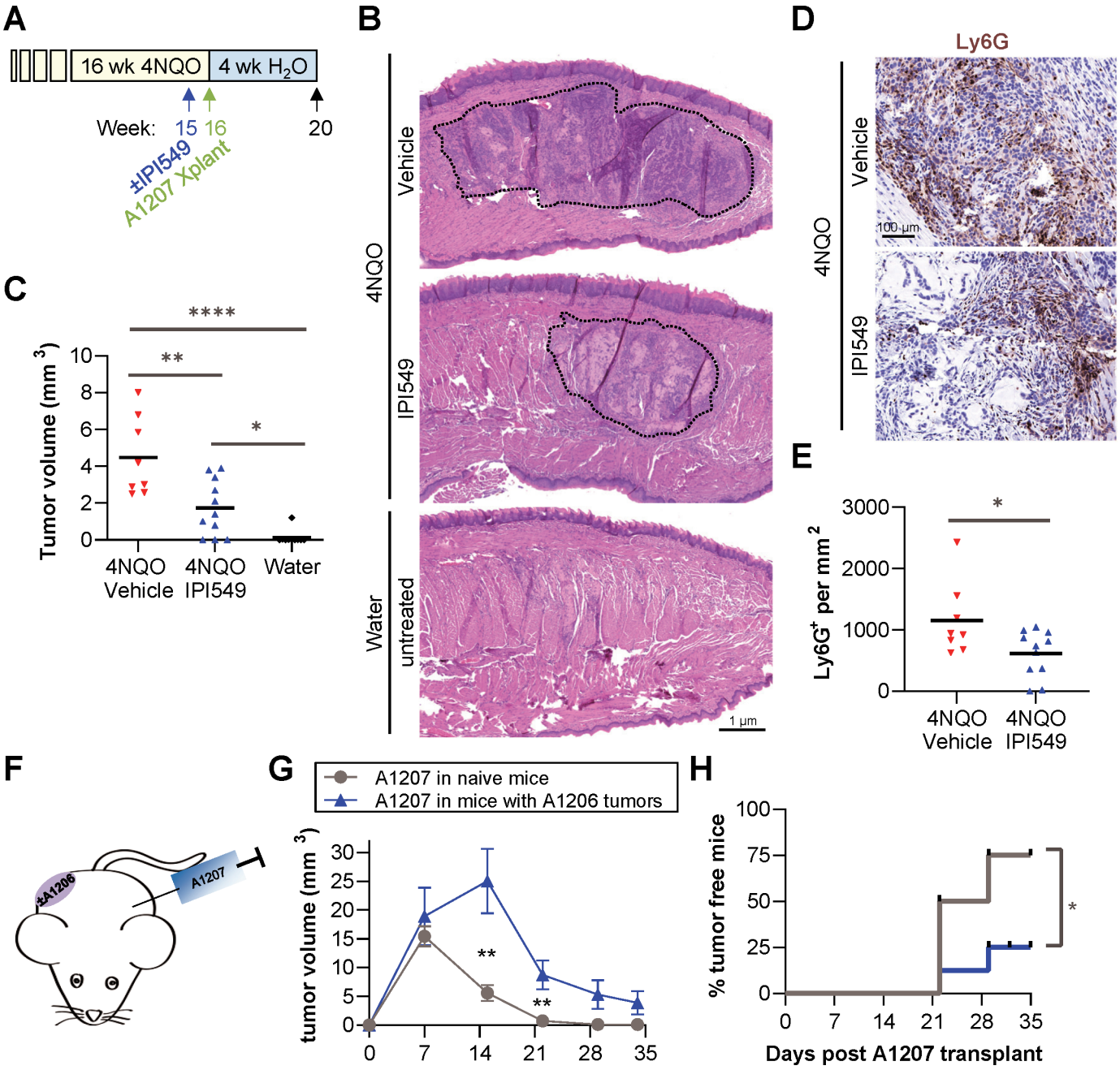

Figure 6 Carcinogenic microenvironment enables A1207 p110γ-dependent tumor growth. (A–E) 4NQO carcinogenesis and treatment regimen: mice received 50 µg/mL 4NQO in the drinking water (or regular drinking water for control mice) for 16 weeks and returned to regular drinking water thereafter. Mice received daily IPI549 or vehicle treatments beginning week 15 for the duration of the experiment and all mice were transplanted with A1207 cells to the dorsal tongue on week 16. (B) Representative images of whole tongue sections from mice treated with water versus 4NQO+IPI549 versus 4NQO+Vehicle all transplanted with A1207 cells on week 16. Black dotted line outlines the tumor border. (C) Tumor volume in each treatment group was determined. *p<0.05, **p<0.01, **p<0.001 determined by one-way ANOVA with Tukey's multiple comparison test (right). (D–E) Ly6G immunostaining and quantification of tongue tumors. *p<0.05 determined by unpaired Student's t-test. (F–H) C57BL/6 mice were transplanted with A1206 tumor cells to the right flank or not transplanted. When A1206 tumors reached 300 mm^3, all mice (naïve and A1206 tumor-bearing) were transplanted with A1207 cells to the left flank. (G) Size of left flank A1207 tumor was monitored over time. Due to the size of A1206 tumors, all mice required euthanasia 34 days after A1207 transplant. **p<0.01 determined by unpaired Student's t-test at the indicated time points. (H) Rate of complete A1207 tumor clearance was monitored over time. *p<0.05 determined by log-rank test. ANOVA, analysis of variance; wk, week; 4NQO, 4-nitroquinoline 1-oxide.

this time point that arises in the tongue surface epithelium and invades into the tongue muscle (online supplemental figure S6). While A1207 tumors failed to grow in tongues of water-treated control mice, tumors were able to grow in 4NQO-treated, vehicle-treated mice. Furthermore, treatment of transplanted 4NQO-treated mice with IPI549 led to

significantly reduced tumor volumes, with 3/11 treated mice exhibiting complete regression (figure 6B,C). This response correlated with Ly6G+ infiltration, as 4NQO-treated mice treated with vehicle exhibited high Ly6G+ cell density in tumors, but Ly6G+ cell density was lower in mice treated with IPI549 (figure 6D,E).

To induce an immunosuppressive microenvironment, we transplanted C57BL/6 mice with A1206 tumors and allowed tumors to reach 300 mm^3, a size at which we previously demonstrated induces systemic (splenic) PMN-MDSC levels and activity compared with wild-type mice (figure 5C). A1207 cells were then transplanted into the contralateral flanks of mice with or without A1206 flank tumors (figure 6F). While the growth of A1206 tumors caused mice to reach humane endpoints and precluded a longer study of the A1207 tumors transplanted to these same mice, we observed significantly larger A1207 tumor volumes at the 14-day and 21-day time points in mice bearing A1206 tumors compared with mice without A1206 tumors (figure 6G). Furthermore, while all A1207 tumors were regressing at the study endpoint in both groups, the rate of complete A1207 tumor regression was reduced threefold in mice bearing A1206 tumors (figure 6H), suggesting that systemic immunosuppression achieved by A1206 tumors may increase A1207 tumorigenesis.

PMN-MDSCs enable tumorigenesis

To directly test whether immunosuppression achieved by PMN-MDSCs could enable tumorigenesis of the poorly tumorigenic A1207 cell line, we co-transplanted A1207 cells with the Ly6G+ cells from wild-type mice or with the Ly6G+ cells from mice bearing A1206 tumors (which function as PMN-MDSCs). A1207 cells co-transplanted with wild-type granulocytes regressed in 75% of mice, while A1207 cells co-transplanted with the granulocytes from A1206 tumor bearing mice regressed in 33% of mice (figure 7) demonstrating that PMN-MDSCs, as a single source of exogenously supplied immunosuppression, are sufficient to dramatically increase A1207 tumorigenesis, which otherwise regress.

DISCUSSION

In contrast to the immunosuppressive microenvironment of HNSCC, studies have shown that premalignant lesions contain a significant infiltration of proinflammatory immune cells such as CD8+ T cells, natural killer cells, and tumor-associated macrophages as well as elevated levels of inflammatory cytokines.[14 33–36] Because immunotherapies generate immune reactivity against the tumor, patients bearing premalignant lesions at high-risk of developing HNSCC may be better candidates for immunotherapy than patients with HNSCC, which typically have immunologically cold tumors.[37] Recent studies support the use of immune checkpoint inhibitors, such as those targeting the Programmed Cell Death Protein 1 (PD-1) and Programmed Cell Death Ligand 1 (PD-L1), (PD1-PDL1) signaling axis, which re-invigorate a cytotoxic T-cell response, as a preventive measure for high-risk premalignant lesions from the 4NQO model.[16 37 38] In addition, the anti-PD1 monoclonal antibody, nivolumab, is currently undergoing phase II clinical trials for use to treat aggressive oral verrucous leukoplakia (ClinicalTrials.gov NCT03692325). Our studies are consistent with those reporting immunological fatigue in premalignant oral lesions.[14 33] Importantly, Chu *et al* previously demonstrated increased CD11b+Gr1+ MDSCs in tongues, spleens, and peripheral blood of 4NQO-treated mice.[39] Our results confirm and build on their findings, demonstrating immunosuppressive functionality of these MDSCs. While Chu *et al* characterized the observed Gr1+ infiltrate as immunosuppressive due to their increased messenger RNA (mRNA) levels of ARG-1 and NOS-2, both of which are involved in MDSC-induced immune suppression,[25 40] our studies showed that Ly6G+ from spleens of tumor-bearing mice suppress T-cell proliferation in vitro, A1207 regression is associated with CD8+ cytotoxic T-cell activity, and spontaneous regression of A1207 transplants can be reduced when A1207 cells are co-transplanted with immunosuppressive PMN-MDSCs. A previous study demonstrated that the 4NQO carcinogenesis model

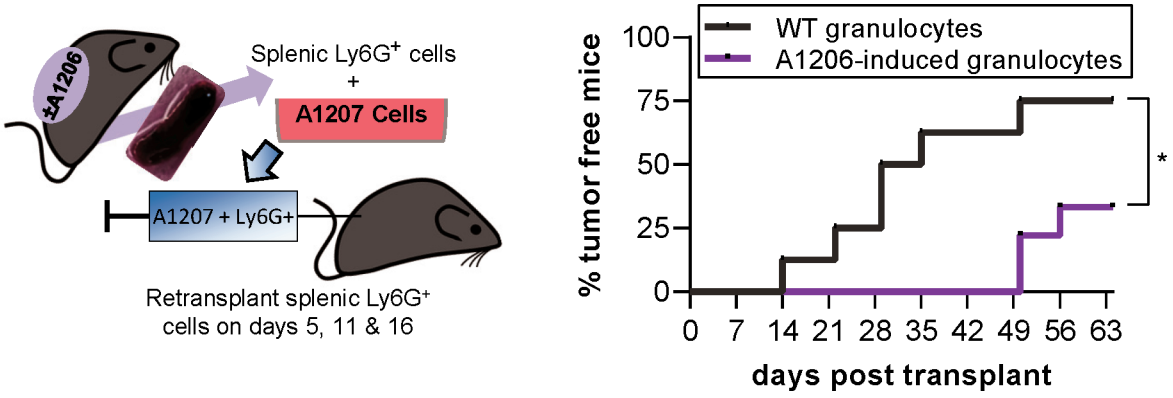

Figure 7 PMN-MDSCs from tumor bearing mice enable A1207 tumor growth. Ly6G+ cells were harvested from spleens of C57BL/6 mice without tumors or bearing A1206 tumors on day 0, 5, 11 and 16. 0.5 million A1207+1.5 million Ly6G+ cells were transplanted to the flanks of recipient C57BL/6 mice on day 0. Initiated tumors were transplanted with another 1.5 million Ly6G+ cells on days 5, 11 and 16. Rate of complete A1207 tumor clearance was monitored over time. *p<0.05 determined by log-rank test. PMN-MDSCs; polymorphonuclear myeloid-derived suppressor cells; WT, wild type.

very closely mimics the mutations induced by tobacco usage and reported Ly6G+ PMN-MDSCs as the highest subpopulation of CD45+ cells in 4NQO-induced tumors, thereby supporting the notion that the 4NQO carcinogenesis model is consistently associated with high Ly6G+ infiltration and an appropriate model of tobacco usage.[20] Our studies revealed that a high amount of Ly6G+ cells are recruited locally to sites of dysplasia in response to tobacco-mimicking mutagenic exposure, where they generate a microenvironment that favors tumor initiation and progression by suppressing CD8+ T-cell proliferation and cytotoxic activity.

PI3Kγ is a myeloid cell specific enzyme critical for the activity of maintaining M2 protumor macrophages and promoting tumor infiltration of immunosuppressive MDSCs.[17] Inhibition of PI3Kγ in preclinical models of HNSCC has been shown to induce antitumor activity and increase the effectiveness of ICB.[17 18] Currently, PI3Kγ inhibitor use in combination with ICB has received Food and Drug Administration Fast Track designation for treating breast cancer and urothelial cancer in clinical trials.[41 42] Our data using a pharmacological inhibitor of PI3Kγ are consistent with a recent report that observed reduced rates of preneoplastic lesions and SCCs induced by 4NQO in the tongues of genetically engineered mice lacking PI3Kγ or expressing a kinase-dead PI3Kγ compared with wild-type C57Bl/6 mice.[43] In addition to reducing progression of dysplasia and preventing tumorigenesis, we also demonstrated that inhibition of PI3Kγ reduces Ly6G+ cell recruitment to sites of dysplasia and that these leukocytes play a critical role in establishing invasive SCC. While studies using PI3Kγ inhibitors have acknowledged an influence on PMN-MDSCs, these studies largely focus on tumor-associated macrophage polarization and activity or a more general effect on tumor-associated myeloid cells broadly.[17 18] Importantly, our data highlight that PI3Kγ signaling in granulocytes is not to be underappreciated. However, because IPI549 has activity against all PI3Kγ-expressing myeloid cells, the effectiveness of IPI549 in chemoprevention likely includes activity against monocytes and macrophages in addition to granulocytes. Taken together, our data demonstrate that high Ly6G+ infiltration may serve as an important predictive biomarker for determining viable patient candidates for immunotherapy and that PI3Kγ inhibitors can be used to prevent HNSCC initiation or progression.

Although the 4NQO model is a robust, controlled, manipulable model of tobacco-induced OSCC, one limitation of our study is the reliance on mouse models, which are subject to inherent differences between human and mouse immune biology. Regarding MDSCs, for example, some mechanisms of immunosuppression used by mouse MDSCs, such as tryptophan and cysteine depletion, have not yet been shown in human MDSCs.[44–46] Furthermore, mouse and human MDSCs differ slightly in their development, most evidently seen in the existence of early-stage MDSCs that lack monocytic or granulocytic markers in humans whereas mice seem to lack this subset of cells entirely.[44] Despite this, both mouse and human MDSC levels are correlated with poor prognoses in OSCC, and share several mechanisms of immunosuppression, such as through inducing oxidative stress and expressing immune checkpoint receptors.[47–52] Additionally, a high neutrophil to lymphocyte ratio is an easy blood-based metric that predicts OSCC, OPMD, and aggressive cancer behavior in human patients,[53–55] thus suggesting that elevated granulocytes in the blood have predictive value in both mice and humans. While human studies are ideal for maximizing opportunities for clinical relevance, there are severely limited opportunities to derive suitable samples from patients with OPMD. Consequently, the use of mouse models, such as the 4NQO model, are essential to provide insight into mechanisms of disease that can then be tested more directly in human trials.

Taken together, our results support therapeutic targeting of granulocytes in tobacco-induced premalignancies, specifically using PI3Kγ inhibitor. Our data, and those of other authors, show that inhibiting PI3Kγ results in an immune microenvironment that is less immunosuppressive. These findings stand to benefit not only patients with OPMDs who are at risk of developing into cancer, but also potentially other high-risk patients such as HNSCC patients that have recently undergone conventional therapy and face greater risk of cancer recurrence due to history of tobacco consumption. As such, there is a strong rationale to exploring the use of PI3Kγ inhibitors for treating premalignancies as a chemopreventive measure. As PI3Kγ inhibition continues to be tested in cancer patient clinical trials, it is crucial to assess affected cell types, identify biomarkers for response prediction, and increase our understanding of immune escape mechanisms. Achieving these goals will guide chemoprevention and therapy choices, ultimately leading to improved patient outcomes.

Acknowledgements The authors thank Pamela Garl for her proofreading of this manuscript and the University of Colorado shared resources for their expertise and technical assistance, which are detailed in the funding section.

Contributors Experiments and data analysis was performed by KAN, LND, YK and CDY. Pathology assessment was performed by LB, VS and AAB. Panel design and supervision was performed by PO. Funding and study supervision was performed by X-JW and CDY. This study was conceived by CDY, the guarantor of this study. The manuscript was written by KAN and CDY with input from all authors, edited by X-JW and approved by all authors.

Funding CY was supported by American Cancer Society IRG #16-184-56 to the University of Colorado Cancer Center and pilot awards from the Cancer League of Colorado (AWD-163274-CY) and the University of Colorado Head and Neck Cancer Research Program. CY and X-JW were supported by SPORE P50CA261605. X-JW was supported by NIH DE24371, DE027329 and DE028420 and VA merit award I01 BX003232. X-JW is the recipient of a Research Career Scientist award (# IK6BX005962) from the Department of Veterans Affairs. Four University of Colorado Cancer Center shared resources used in this study (Comparative Pathology, Flow Cytometry, Pathology, Human Immunology Monitoring (RRID:SCR_021985)) were funded in part by Cancer Center Support Grant P30CA046934.

Competing interests None declared.

Patient consent for publication Not applicable.

Ethics approval All animal work was performed in accordance with protocols approved by the University of Colorado Anschutz Medical Campus Institutional Animal Care and Use Committee (IACUC). Protocols 254 and 1223.

Provenance and peer review Not commissioned; externally peer reviewed.

Data availability statement Data are available upon reasonable request. Data and materials are available upon reasonable request made to the corresponding author.

ORCID iD

Christian D Young http://orcid.org/0000-0001-9846-488X

REFERENCES

1 Ferlay J, Colombet M, Soerjomataram I, *et al*. Estimating the global cancer incidence and mortality in 2018: GLOBOCAN sources and methods. *Int J Cancer* 2019;144:1941–53. 10.1002/ijc.31937 Available: https://onlinelibrary.wiley.com/toc/10970215/144/8
2 Bray F, Ferlay J, Soerjomataram I, *et al*. Global cancer Statistics 2018: GLOBOCAN estimates of incidence and mortality worldwide for 36 cancers in 185 countries. *CA Cancer J Clin* 2018;68:394–424.
3 Johnson DE, Burtness B, Leemans CR, *et al*. Head and neck squamous cell carcinoma. *Nat Rev Dis Primers* 2020;6:92.
4 Burtness B, Harrington KJ, Greil R, *et al*. Pembrolizumab alone or with chemotherapy versus Cetuximab with chemotherapy for recurrent or metastatic squamous cell carcinoma of the head and neck (KEYNOTE-048): a randomised, open-label, phase 3 study. *Lancet* 2019;394:1915–28.
5 Ferris RL, Blumenschein G Jr, Fayette J, *et al*. Nivolumab for recurrent squamous-cell carcinoma of the head and neck. *N Engl J Med* 2016;375:1856–67.
6 Harrington KJ, Ferris RL, Blumenschein G, *et al*. Nivolumab versus standard, single-agent therapy of investigator's choice in recurrent or metastatic squamous cell carcinoma of the head and neck (Checkmate 141): health-related quality-of-life results from a randomised, phase 3 trial. *Lancet Oncol* 2017;18:1104–15.
7 Ranganathan K, Kavitha L. Oral epithelial dysplasia: classifications and clinical relevance in risk assessment of oral potentially malignant disorders. *J Oral Maxillofac Pathol* 2019;23:19–27.
8 Ang KK, Harris J, Wheeler R, *et al*. Human Papillomavirus and survival of patients with oropharyngeal cancer. *N Engl J Med* 2010;363:24–35.
9 Lassen P, Huang SH, Su J, *et al*. Treatment outcomes and survival following definitive (Chemo)Radiotherapy in HPV-positive oropharynx cancer: large-scale comparison of DAHANCA vs PMH cohorts. *Int J Cancer* 2022;150:1329–40.
10 Iocca O, Sollecito TP, Alawi F, *et al*. Potentially malignant disorders of the oral cavity and oral dysplasia: A systematic review and meta-analysis of malignant transformation rate by subtype. *Head & Neck* 2020;42:539–55. 10.1002/hed.26006 Available: https://onlinelibrary.wiley.com/toc/10970347/42/3
11 Mello FW, Miguel AFP, Dutra KL, *et al*. Prevalence of oral potentially malignant disorders: A systematic review and meta-analysis. *J Oral Pathol Med* 2018;47:633–40.
12 Pardoll DM. The blockade of immune checkpoints in cancer Immunotherapy. *Nat Rev Cancer* 2012;12:252–64.
13 Wei SC, Duffy CR, Allison JP. Fundamental mechanisms of immune Checkpoint blockade therapy. *Cancer Discov* 2018;8:1069–86.
14 Woodford D, Johnson SD, De Costa A-MA, *et al*. An inflammatory cytokine milieu is prominent in Premalignant oral lesions, but subsides when lesions progress to squamous cell carcinoma. *J Clin Cell Immunol* 2014;5:230.
15 Mittal D, Gubin MM, Schreiber RD, *et al*. New insights into cancer Immunoediting and its three component phases--elimination, equilibrium and escape. *Curr Opin Immunol* 2014;27:16–25.
16 Wang J, Xie T, Wang B, *et al*. PD-1 blockade prevents the development and progression of carcinogen-induced oral Premalignant lesions. *Cancer Prevention Research* 2017;10:684–93.
17 Kaneda MM, Messer KS, Ralainirina N, *et al*. Corrigendum: Pi3Kγ is a molecular switch that controls immune suppression. *Nature* 2017;542:124.
18 De Henau O, Rausch M, Winkler D, *et al*. Overcoming resistance to Checkpoint blockade therapy by targeting Pi3Kgamma in myeloid cells. *Nature* 2016;539:443–7.
19 Tang X-H, Knudsen B, Bemis D, *et al*. Oral cavity and Esophageal carcinogenesis modeled in carcinogen-treated mice. *Clin Cancer Res* 2004;10:301–13.
20 Wang Z, Wu VH, Allevato MM, *et al*. Syngeneic animal models of tobacco-associated oral cancer reveal the activity of in situ anti-CTLA-4. *Nat Commun* 2019;10:5546.
21 Yamaguchi H, Hiroi M, Mori K, *et al*. Simultaneous expression of Th1- and Treg-associated Chemokine genes and Cd4(+), Cd8(+), and Foxp3(+) cells in the Premalignant lesions of 4Nqo-induced Mouse tongue tumorigenesis. *Cancers* 2021;13:1835.
22 Sequeira I, Rashid M, Tomás IM, *et al*. Genomic landscape and Clonal architecture of Mouse oral squamous cell Carcinomas dictate tumour Ecology. *Nat Commun* 2020;11:5671.
23 Chadwick JW, Macdonald R, Ali AA, *et al*. Tnfalpha signaling is increased in progressing oral potentially malignant disorders and regulates malignant transformation in an oral carcinogenesis model. *Front Oncol* 2021;11:741013.
24 Wengner AM, Pitchford SC, Furze RC, *et al*. The coordinated action of G-CSF and ELR + CXC Chemokines in neutrophil mobilization during acute inflammation. *Blood* 2008;111:42–9.
25 Gabrilovich DI, Ostrand-Rosenberg S, Bronte V. Coordinated regulation of myeloid cells by tumours. *Nat Rev Immunol* 2012;12:253–68.
26 Fruman DA, Chiu H, Hopkins BD, *et al*. The Pi3K pathway in human disease. *Cell* 2017;170:605–35.
27 Vanhaesebroeck B, Perry MWD, Brown JR, *et al*. Pi3K inhibitors are finally coming of age. *Nat Rev Drug Discov* 2021;20:741–69.
28 Evans CA, Liu T, Lescarbeau A, *et al*. Discovery of a selective Phosphoinositide-3-kinase (Pi3K)-Gamma inhibitor (IPI-549) as an Immuno-oncology clinical candidate. *ACS Med Chem Lett* 2016;7:862–7.
29 Vitale-Cross L, Molinolo AA, Martin D, *et al*. Metformin prevents the development of oral squamous cell Carcinomas from carcinogen-induced Premalignant lesions. *Cancer Prev Res (Phila)* 2012;5:562–73.
30 White RA, Neiman JM, Reddi A, *et al*. Epithelial stem cell mutations that promote squamous cell carcinoma metastasis. *J Clin Invest* 2013;123:4390–404.
31 Strait AA, Woolaver RA, Hall SC, *et al*. Distinct immune Microenvironment profiles of therapeutic responders emerge in combined Tgfbeta/PD-L1 blockade-treated squamous cell carcinoma. *Commun Biol* 2021;4:1005.
32 Bronte V, Brandau S, Chen S-H, *et al*. Recommendations for myeloid-derived Suppressor cell nomenclature and characterization standards. *Nat Commun* 2016;7:12150.
33 De Costa A-MA, Schuyler CA, Walker DD, *et al*. Characterization of the evolution of immune phenotype during the development and progression of squamous cell carcinoma of the head and neck. *Cancer Immunol Immunother* 2012;61:927–39.
34 Bondad-Palmario GG. Histological and Immunochemical studies of oral Leukoplakia: phenotype and distribution of immunocompetent cells. *J Philipp Dent Assoc* 1995;47:3–18.
35 Mori K, Haraguchi S, Hiori M, *et al*. Tumor-associated Macrophages in oral Premalignant lesions Coexpress Cd163 and Stat1 in a Th1-dominated Microenvironment. *BMC Cancer* 2015;15:573.
36 Stasikowska-Kanicka O, Wągrowska-Danilewicz M, Danilewicz M. Cd8+ and Cd163+ infiltrating cells and PD-L1 Immunoexpression in oral Leukoplakia and oral carcinoma. *APMIS* 2018;126:732–8.
37 Levingston CA, Young MRI. Transient immunological and clinical effectiveness of treating mice bearing Premalignant oral lesions with PD-1 antibodies. *Int J Cancer* 2017;140:1609–19. 10.1002/ijc.30543 Available: http://doi.wiley.com/10.1002/ijc.v140.7
38 Shi Y, Xie T, Leach DG, *et al*. Local anti-PD-1 delivery prevents progression of Premalignant lesions in a 4Nqo-oral carcinogenesis mouse model. *Cancer Prevention Research* 2021;14:767–78.
39 Chu M, Su Y-X, Wang L, *et al*. Myeloid-derived Suppressor cells contribute to oral cancer progression in 4Nqo-treated mice. *Oral Dis* 2012;18:67–73.
40 Bronte V, Serafini P, De Santo C, *et al*. IL-4-induced Arginase 1 suppresses Alloreactive T cells in tumor-bearing mice. *J Immunol* 2003;170:270–8.

41 Infinity receives fast track designation for Eganelisib in combination with a Checkpoint inhibitor and chemotherapy for first-line treatment of advanced TNBC.;Press release September 29, 2020. n.d. Available: https://bit.ly/3imQjYR
42 FDA grants IPI-549 and Nivolumab combo fast track designation for urothelial cancer. press release March 25, 2020. n.d. Available: https://www.targetedonc.com/view/sequential-mitomycin-with-bcg-is-shown-to-be-safe-in-high-risk-nmibc
43 Berta GN, Di Scipio F, Yang Z, *et al*. n.d. Chemical oral Cancerogenesis is impaired in Pi3Kgamma knockout and kinase-dead mice. *Cancers*;13:4211.
44 Vanhaver C, van der Bruggen P, Bruger AM. MDSC in mice and men: mechanisms of immunosuppression in cancer. *J Clin Med* 2021;10:2872:13.:.
45 Srivastava MK, Sinha P, Clements VK, *et al*. Myeloid-derived Suppressor cells inhibit T-cell activation by Depleting Cystine and Cysteine. *Cancer Res* 2010;70:68–77.
46 Platten M, Wick W, Van den Eynde BJ. Tryptophan catabolism in cancer: beyond IDO and Tryptophan depletion. *Cancer Res* 2012;72:5435–40.
47 Shojaei F, Wu X, Qu X, *et al*. G-CSF-initiated myeloid cell mobilization and angiogenesis mediate tumor Refractoriness to anti-VEGF therapy in Mouse models. *Proc Natl Acad Sci U S A* 2009;106:6742–7.
48 Wang P-F, Song S-Y, Wang T-J, *et al*. Prognostic role of pretreatment circulating Mdscs in patients with solid malignancies: A meta-analysis of 40 studies. *Oncoimmunology* 2018;7:e1494113.
49 Liu C-Y, Wang Y-M, Wang C-L, *et al*. Population alterations of L-Arginase- and inducible nitric oxide synthase-expressed Cd11B+/Cd14⁻/Cd15+/Cd33+ myeloid-derived Suppressor cells and Cd8+ T lymphocytes in patients with advanced-stage non-small cell lung cancer . *J Cancer Res Clin Oncol* 2010;136:35–45.
50 Corzo CA, Cotter MJ, Cheng P, *et al*. Mechanism regulating reactive oxygen species in tumor-induced myeloid-derived Suppressor cells. *J Immunol* 2009;182:5693–701.
51 Lu C, Redd PS, Lee JR, *et al*. The expression profiles and regulation of PD-L1 in tumor-induced myeloid-derived Suppressor cells. *OncoImmunology* 2016;5:e1247135.
52 Gebhardt C, Sevko A, Jiang H, *et al*. Myeloid cells and related chronic inflammatory factors as novel predictive markers in Melanoma treatment with Ipilimumab. *Clin Cancer Res* 2015;21:5453–9.
53 Howard R, Kanetsky PA, Egan KM. Exploring the Prognostic value of the neutrophil-to-lymphocyte ratio in cancer. *Sci Rep* 2019;9:19673.
54 Hasegawa T, Iga T, Takeda D, *et al*. Neutrophil-lymphocyte ratio associated with poor prognosis in oral cancer: a retrospective study. *BMC Cancer* 2020;20:568.
55 Singh S, Singh J, Ganguly R, *et al*. Diagnostic efficacy of neutrophil to lymphocyte ratio (NLR) in oral potentially malignant disorders and oral cancer. *Indian J Pathol Microbiol* 2021;64:243–9.